RECORDSOF CHEMICAL SCIENCES

Synthesis, Structural Characterization, and Antimicrobial Activity of Fe(III), Co(II), and Ni(II) Complexes with Quercetin and 2-Aminothiazole

[1]*Abdullahi O. Rajee, [1]Kareemat T. Adesope , [2]Saadu O. Haizat, [3]Abdulbasit A. Aliyu, [4]Sheriff O. Ayinla, [1]Rabiat H. Ibrahim, and [1]Omotola E. Tajudeen

Accepted: 23th Nov, 2025
Published: 02th Dec., 2025

https://doi.org/10.33003/frscs-2025-0404/03

1. Department of Chemistry, Faculty of Physical Sciences, University of Ilorin, Kwara, Nigeria.
2. Department of Chemistry and Industrial Chemistry, Faculty of Pure and Applied Sciences, Kwara State University, Malete, PMB 1530, Ilorin, Kwara State, Nigeria.
3. Department of Pure & Industrial Chemistry, Kogi State University, Anyigba, Kogi, Nigeria.
4. Department of Chemical and Geological Sciences, Al-Hikmah University, Ilorin, Nigeria.
**Corresponding Author:*
Abdullahi O. Rajee
olarajee@unilorin.edu.ng

FRsCS Vol.4 No. 4 (2025)
Official Journal of Dept. of Chemistry, Federal University of Dutsin-Ma, Katsina State.
http://rudmafudma.com

ISSN (Online): 2705-2362
ISSN (Print): 2705-2354

Abstract

Mixed-ligand complexes of quercetin (QUE) and 2-aminothiazole (2-AMT) with Fe(III), Co(II), and Ni(II) ions were synthesized via a solvothermal reflux route using a 1:1:1 metal-to-ligand ratio. The complexes, formulated as $[M(QUE)(2\text{-}AMT)(H_2O)_2]$ (M = Fe, Co, Ni), were characterized by elemental analysis, UV–Visible Spectroscopy, and FT–IR spectroscopy. Spectral data confirmed bidentate coordination of QUE through its carbonyl and hydroxyl oxygen atoms and of 2-AMT via the endocyclic nitrogen, consistent with octahedral geometry around the metal centers. The complexes exhibited low molar conductivities (15–25 Ω^{-1} cm^2 mol^{-1}), indicating their non-electrolytic nature and neutral stoichiometry. Antimicrobial activity was assessed against *Staphylococcus aureus, Escherichia coli, Klebsiella pneumoniae, Pseudomonas aeruginosa,* and *Aspergillus niger* using the agar well diffusion method. All complexes showed enhanced activity compared to the free ligands, with the Co(II) complex displaying the highest potency (22 mm inhibition zone against P. aeruginosa, MIC = 75 µg/mL). The observed enhancement is attributed to increased lipophilicity and metal–ligand synergism that facilitates microbial membrane penetration. These findings underscore the potential of quercetin–2-aminothiazole coordination frameworks as promising scaffolds for metal-based antimicrobial drug design.

Keywords: Quercetin, Aminothiazole, Metal Complexes, Antimicrobial

Introduction

Flavonoids constitute a diverse class of naturally occurring polyphenolic compounds widely distributed in plants, fruits, and beverages. Among them, quercetin (3, 3′, 4′, 5, 7-pentahydroxyflavone) has received extensive attention due to its potent antioxidant, anti-inflammatory, anticancer, and antimicrobial activities (Garg et al., 2019; Chagas et al., 2022; Imai et al., 2017). Structurally, quercetin possesses a C6–C3–C6 flavonoid skeleton with multiple hydroxyl groups and a conjugated carbonyl system that facilitates electron delocalization and metal chelation through its 3-hydroxy-4-carbonyl and 5-hydroxy-4-carbonyl sites (Al-Sehemi et al., 2016; Ramzan et al., 2025). The ability of quercetin to coordinate with transition metals has been exploited to develop metal-based therapeutics and catalytic systems with enhanced redox and biological properties (Kasprzak et al., 2015; Refat et al., 2021; Stefanache et al., 2025). Transition metal complexes remain a cornerstone of medicinal inorganic chemistry, offering unique electronic and structural versatility. Coordination of bioactive ligands to metals such as Fe(III), Co(II), and Ni(II) can modulate solubility, lipophilicity, and redox potential, thereby influencing their biological performance

(Ayinla *et al.*, 2024; Bale *et al.*, 2022; Rajee *et al.*, 2020). Previous studies have demonstrated that metal–flavonoid complexes often display improved antioxidant or antimicrobial activity relative to the free ligands, attributable to metal-mediated charge transfer and enhanced membrane permeability (Rajee *et al.*, 2024, 2022; Yaraki *et al.*, 2022).

Heterocyclic compounds containing nitrogen and sulphur atoms, particularly thiazole derivatives, are also well recognized for their pharmacological significance (Kapoor *et al.*, 2025). 2-Aminothiazole, a key heterocyclic scaffold, exhibits diverse biological activities including antimicrobial, anticancer, and enzyme inhibitory properties (Obaleye *et al.*, 2014; Kapoor *et al.*, 2025). Its coordination through the endocyclic nitrogen further enhances its capacity to form stable and biologically active metal complexes (Thakur *et al.*, 2025). Despite numerous reports on individual quercetin–metal and 2-aminothiazole–metal complexes, the synergistic combination of these two ligands within a single coordination framework remains largely unexplored. Such hybridisation could yield mixed-ligand complexes with complementary functionalities—quercetin providing antioxidant and chelating strength, and 2-aminothiazole contributing nitrogen–sulphur donor flexibility and pharmacophoric activity.

The rising challenge of antimicrobial resistance (AMR) underscores the urgent need for new therapeutic agents capable of overcoming multidrug-resistant pathogens ((Farajzadeh Öztürk *et al.*, 2025). Metal-based systems offer a promising route, as their modes of action often involve redox activity, reactive oxygen species generation, and enzyme inhibition—mechanisms distinct from those of conventional antibiotics (Hadi & Jamel, 2025; AL-Ghamdi, 2025).

In this study, we report the synthesis, spectral characterization, and antimicrobial evaluation of novel Fe(III), Co(II), and Ni(II) complexes containing both quercetin and 2-aminothiazole ligands. The selection of Fe(III), Co(II), and Ni(II) was deliberate and driven by their distinct electronic and redox properties that directly influence antimicrobial performance. Fe(III) (high-spin d^5) is strongly redox-active and capable of generating cytotoxic reactive oxygen species (ROS) via Fenton-type reactions, a mechanism widely exploited in metallodrugs (Matesanz *et al.*, 2021; Wani *et al.*, 2023). Co(II) (high-spin d^7) offers flexible coordination geometry, high lipophilicity upon chelation, and facile Co(II)/Co(III) redox cycling under physiological conditions, which frequently results in superior antimicrobial activity in cobalt–flavonoid and cobalt–heterocyclic complexes (AL-Ghamdi, 2025; Göktürk, 2025). Ni(II) (d^8), in contrast, forms stable octahedral complexes with moderate redox activity and is particularly effective at inhibiting microbial enzymes such as urease and hydrogenase through strong ligand-field stabilization (Alhussaini *et al.*, 2025; Abdou, 2025). Studying these three adjacent first-row transition metals with an identical ligand set therefore enables a systematic evaluation of how d-electron count, spin state, and redox potential modulate lipophilicity, ROS generation, enzyme inhibition, and overall antimicrobial efficacy—critical parameters for the rational design of next-generation metal-based therapeutic agents.

The coordination behaviour was elucidated using UV–Visible and FT–IR spectroscopy, while the antimicrobial assays established correlations between structural features and biological performance. The study aims to provide new insights into the structure–activity relationship of flavonoid–thiazole mixed-ligand metal complexes, contributing to the rational design of metal-based antimicrobial agents, addressing the urgent need for effective therapies against resistant pathogens.

Experimental

Materials and Reagents

Quercetin hydrate and 2-aminothiazole were obtained from Sigma-Aldrich (analytical grade) and used without further purification.

Metal salts, including ferric nitrate nonahydrate [$Fe(NO_3)_3 \cdot 9H_2O$], cobalt(II) nitrate hexahydrate [$Co(NO_3)_2 \cdot 6H_2O$], and nickel(II) nitrate hexahydrate [$Ni(NO_3)_2 \cdot 6H_2O$], were procured from the Chemistry Laboratory, University of Ilorin, Nigeria. Sodium hydroxide (NaOH), ethanol, dimethyl sulfoxide (DMSO), and n-hexane were of analytical grade. Distilled water was obtained from the Central Research Laboratories, University of Ilorin.

General Procedure for the Synthesis of Metal Complexes

Mixed-ligand metal complexes of quercetin (QUE) and 2-aminothiazole (2-AMT) were synthesised following a modified literature method (Ayinla *et al.*, 2024) using a 1:1:1 molar ratio of metal salt, quercetin, and 2-aminothiazole.

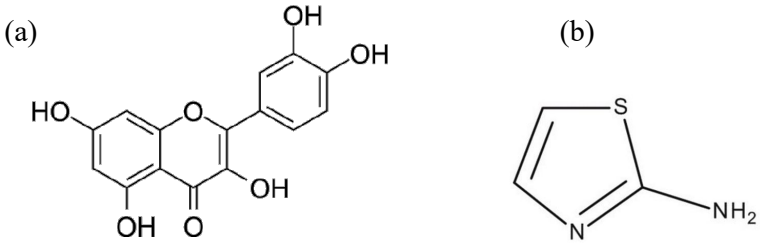

Figure 1: Chemical Structures of Ligands **(a)** Quercetin **(b)** 2-aminothiazole

In a typical synthesis, quercetin hydrate (2.10 mmol) and the corresponding metal nitrate (2.00 mmol) were dissolved in 25 mL of ethanol and refluxed at 80 °C for 30 min to facilitate initial coordination. A separate ethanolic solution of 2-aminothiazole (2.10 mmol, 5 mL) was added dropwise to the refluxing mixture, and the solution was stirred under reflux for an additional 4 h. The reaction mixture was neutralised with dilute NaOH to pH ≈ 7, allowed to stand at room temperature, and the resulting precipitate was filtered, washed sequentially with ethanol and distilled water, and air-dried. The reaction scheme illustrating the synthesis of the mixed-ligand complexes [M(QUE)(2-AMT)(H_2O)$_2$] (M = Fe(III), Co(II), Ni(II)) is provided in Figure 2.

Synthesis of [Fe(QUE)(2-AMT)(H_2O)$_2$] (Complex 1)

Yield: 0.691 g (70.12%). Anal. Calcd for $C_{18}H_{18}FeN_2O_9S_2$ (MW 492.24 g/mol): C, 43.92; H, 3.28; N, 5.69. Found: C, 43.15; H, 3.54; N, 5.98. IR (DMSO, cm^{-1}): 3417.98 (br, O–H), 1651.12 (s, C=O), 1481.38 (s, C=N), 1593.25 (m, C=C), 628.81–516.94 (w, M–O, M–N). UV-Vis (DMSO, λ_max, nm): 301, 405, 514.

Synthesis of [Co(QUE)(2-AMT)(H_2O)$_2$] (Complex 2)

Yield: 0.686 g (69.23%). Anal. Calcd for $C_{18}H_{18}CoN_2O_9S_2$ (MW 495.33 g/mol): C, 43.65; H, 3.26; N, 5.66. Found: C, 43.42; H, 3.37; N, 5.51. IR (DMSO, cm^{-1}): 3417.98 (br, O–H), 1635.69 (s, C=O), 1508.38 (s, C=N), 1558.54 (m, C=C), 636.53–520.80 (w, M–O, M–N). UV-Vis (DMSO, λ_max, nm): 300, 406, 454, 503.

Synthesis of [Ni(QUE)(2-AMT)(H_2O)$_2$] (Complex 3)

Yield: 0.705 g (71.31%). Anal. Calcd for $C_{18}H_{18}NiN_2O_9S_2$ (MW 493.99 g/mol): C, 43.67; H, 3.26; N, 5.66. Found: C, 43.46; H, 3.28; N, 5.64. IR (DMSO, cm^{-1}): 3417.98 (br, O–H), 1620.26 (s, C=O), 1508.38 (s, C=N), 1431.23 (m, C=C), 698.25–621.10 (w, M–O, M–N). UV-Vis (DMSO, λ_max, nm): 300, 400, 501.

Physical and Spectroscopic Measurements

Melting points were determined using a Stuart SMP30 melting point apparatus. Elemental analyses (C, H, N) were performed on a Perkin-Elmer Series II 2400 CHNS/O analyser. FT-IR spectra were recorded as KBr pellets on a Perkin-Elmer GX-FT/IR spectrometer in the range 4000–400 cm^{-1}.

UV–Visible spectra were measured in DMSO on a Shimadzu UV-3600 Plus spectrophotometer (200–800 nm). Magnetic susceptibility measurements were carried out at 298 K by the Gouy method using a Sherwood Scientific MK I magnetic susceptibility balance calibrated with $Hg[Co(SCN)_4]$. Effective magnetic moments (μ_eff) were calculated after applying diamagnetic corrections using Pascal's constants. Molar conductance of 10^{-3} M solutions in DMSO was measured at 25 ± 1 °C using a Jenway 4310 conductivity meter.

Antimicrobial Activity

The antimicrobial activity of the ligands and metal complexes was evaluated using the agar well diffusion method (Pravin & Raman, 2013) against *Staphylococcus aureus* ATCC 25923 (Gram-positive), *Escherichia coli* ATCC 25922 (Gram-negative), *Klebsiella pneumoniae* ATCC 700603 (Gram-negative), and *Pseudomonas aeruginosa* ATCC 27853 (Gram-negative), as well as the fungus *Aspergillus niger* ATCC 16888 (fungus). Test solutions were prepared in DMSO at concentrations of 25, 50, 100, and 200 µg/mL. Wells (5 mm diameter) were loaded with 0.1 mL of each sample, and plates were incubated at 37 °C for 24 h for bacteria or at room temperature for 48 h for fungi. Zones of inhibition (mm) were measured, and the minimum inhibitory concentration (MIC) was determined as the lowest concentration preventing visible growth. All experiments were performed in triplicate.

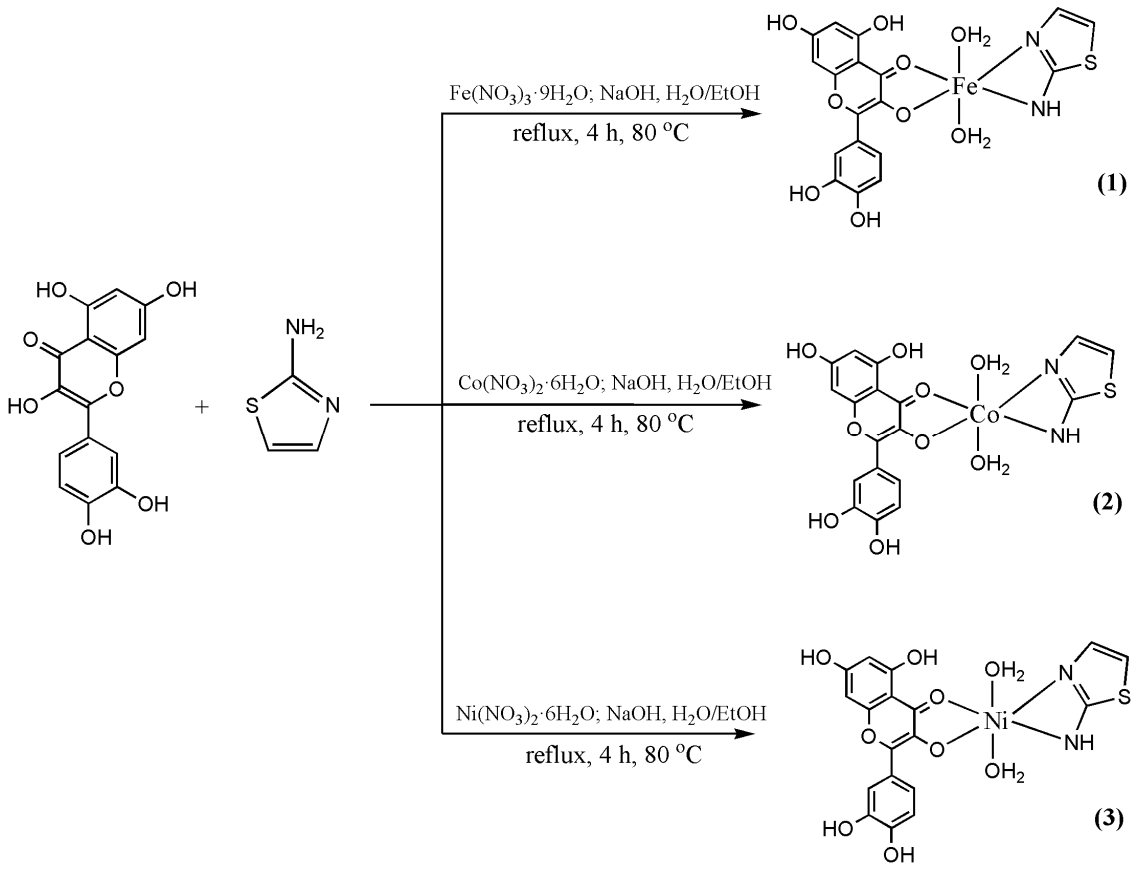

Figure 2: Reaction Scheme for the synthesis of complexes

Results and Discussion

Physicochemical Properties

The physicochemical properties of the synthesized mixed-ligand metal complexes, [M(QUE)(2-AMT)(H_2O)$_2$] (where M = Fe, Co, Ni), were investigated to elucidate their coordination behaviour, stability, and electronic features. Data on yield, colour, melting point, elemental composition, and molar conductivity are summarized in Table 1.

General Observations

All complexes were obtained as stable, coloured solids with good yields (69–71%), indicating efficient complexation between quercetin and 2-aminothiazole ligands. The colours varied from black (Fe(III) and Co(II) complexes) to deep orange (Ni(II) complex), consistent with their respective d-electron configurations and ligand-field transitions. The dark colour of the Fe(III) complex is characteristic of high-spin d^5 systems exhibiting spin-allowed charge-transfer bands, while the orange hue of the Ni(II) complex aligns with d–d transitions typical of octahedral d^8 species (Abraham & Acree, 2014; Ai & Lu, 2025). Such colour variations support the presence of ligand-to-metal charge transfer (LMCT) and d–d excitations, later confirmed by UV–Vis spectroscopy.

Solubility and Thermal Stability

The complexes were insoluble in water, ethanol, and n-hexane, but soluble in hot DMSO, reflecting their neutral nature and high lattice stability. The limited solubility in common solvents arises from extensive chelation and increased molecular rigidity following coordination. The observed melting points (320–335 °C) were significantly higher than those of the free ligands, confirming enhanced thermal stability due to metal–ligand bond formation and increased lattice energy within the chelated framework (Mohammed *et al.*, 2025).

Molar Conductivity

Molar conductivity measurements in 10^{-3} M DMSO solutions gave values between 15–25 Ω^{-1} cm^2 mol^{-1}, indicative of non-electrolytic behaviour. These results confirm that nitrate ions are not present as free counterions but are likely replaced or neutralized during complex formation, resulting in neutral molecular species (Woźnicka *et al.*, 2025). The absence of ionic conduction is consistent with the proposed formulation [M(QUE)(2-AMT)(H_2O)$_2$].

Elemental Analysis

The experimental C, H, and N percentages closely matched the calculated values for the proposed stoichiometry [M(QUE)(2-AMT)(H_2O)$_2$], confirming the successful incorporation of both ligands in a 1:1:1 ratio. The small deviations (< 0.5%) between theoretical and experimental values are within acceptable analytical limits and further support the purity and correct formulation of the complexes.

Magnetic Susceptibility

Magnetic moment values were consistent with high-spin octahedral geometries for all complexes. The Fe(III) complex exhibited μ_{eff} = 5.92 BM (five unpaired electrons, d^5), the Co(II) complex μ_{eff} = 4.80 BM (three unpaired electrons, d^7), and the Ni(II) complex μ_{eff} = 2.90 BM (two unpaired electrons, d^8). These values agree with expected spin-only moments for octahedral high-spin configurations (McMills *et al.*, 2014), confirming the electronic assignments inferred from their UV–Vis spectra.

The combined physicochemical data—including solubility, melting point, conductivity, and magnetic measurements—support the formation of neutral, thermally stable, high-spin octahedral mixed-ligand metal complexes. The observed colour variations correlate with metal ion oxidation states and ligand-field effects, affirming successful coordination through both oxygen (quercetin) and nitrogen (2-aminothiazole) donor atoms. These physicochemical properties collectively confirm the formation of stable, octahedral mixed-ligand complexes with distinct coordination characteristics compared to the free ligands.

FTIR Spectral Analysis

The FTIR spectra of quercetin (QUE), 2-aminothiazole (2-AMT), and their mixed-ligand metal complexes [M(QUE)(2-AMT)(H_2O)$_2$] (M = Fe, Co, Ni) were recorded in the 4000–400 cm^{-1} range to identify the functional groups involved in coordination. Characteristic absorption bands and their assignments are summarized in **Table 2**.

The free quercetin spectrum displayed a broad O–H stretching band at 3405 cm^{-1} and a strong ν(C=O) band at 1664 cm^{-1}, corresponding to the carbonyl group of the γ-pyrone ring. Bands at 1611 cm^{-1} (C=C), 1381 cm^{-1} (C–O–H), and 1261 cm^{-1} (C–O–C) are characteristic of the flavonoid skeleton (Hassan *et al.*, 2025). For 2-aminothiazole, absorptions at 3413 cm^{-1} (N–H stretch) and 1520 cm^{-1} (C=N) confirmed the thiazole and amino functionalities.

Upon complexation, significant spectral shifts were observed. The ν(C=O) band of quercetin shifted to lower frequencies (1620–1651 cm^{-1}), indicating coordination through the carbonyl oxygen. The ν(C=N) band of 2-AMT shifted from 1520 to 1481–1508 cm^{-1}, consistent with metal–nitrogen bonding. The O–H band remained broad around 3418 cm^{-1} but with reduced intensity, suggesting the presence of coordinated water molecules rather than lattice water (Amin *et al.*, 2025). Weak new absorptions between 520–700 cm^{-1} were assigned to ν(M–O) and ν(M–N) vibrations, confirming metal–ligand coordination (Bogatinovska *et al.*, 2025). Small downward shifts in ν(C=C) and ν(C–O–C) frequencies imply electronic delocalization through π-back donation and redistribution of charge density within the aromatic system. Collectively, these features confirm that quercetin acts as a bidentate O,O-donor via its carbonyl and phenolic groups, while 2-aminothiazole coordinates through the endocyclic nitrogen. Two coordinated water molecules complete the octahedral geometry proposed for the complexes. FTIR evidence supports mixed O- and N-donor coordination, confirming chelation through carbonyl oxygen, phenolic oxygen, and thiazole nitrogen atoms. The persistence of broad O–H stretching bands near 3400 cm^{-1} signifies the presence of coordinated water molecules rather than lattice-held water, aligning with the proposed [M(QUE)(2-AMT)(H_2O)$_2$] formulation.

Electronic Spectral Analysis

The UV–Vis spectra of the ligands and their complexes were recorded in DMSO to explore electronic transitions and infer coordination geometry (Figure 3). Relevant absorption bands and their assignments are given in **Table 3**. Quercetin exhibited two main absorption bands at 250 nm and 370 nm, corresponding to π→π* and n→π* transitions within the conjugated flavonoid system. 2-Aminothiazole showed a single strong π→π* transition near 255 nm associated with the thiazole ring.

Upon coordination, new bands appeared in the visible region (400–520 nm), attributed to d–d transitions and ligand-to-metal charge-transfer (LMCT) bands. The Fe(III) complex showed bands at 301 nm (LMCT), 405 nm, and 514 nm ($^6A_1g \rightarrow {}^4T_2g$, $^6A_1g \rightarrow {}^4T_1g$ transitions), consistent with a high-spin octahedral d^5 configuration (Kumar *et al.*, 2025). The Co(II) complex exhibited absorptions at 300, 406, 454, and 503 nm, corresponding to $^4T_1g(F) \rightarrow {}^4T_1g(P)$, $^4T_1g(F) \rightarrow {}^4A_2g$, and $^4T_1g(F) \rightarrow {}^4T_2g(F)$ transitions typical of octahedral Co(II) complexes. The Ni(II) complex displayed bands at 300, 400, and 501 nm, assigned to $^3A_2g(F) \rightarrow {}^3T_2g(P)$ and $^3A_2g(F) \rightarrow {}^3T_1g(F)$ transitions characteristic of octahedral d^8 systems (Göktürk, 2025; Abdou, 2025).

The molar absorptivity (ε) values were in the range of 2.5–4.5 × 10^3 L mol^{-1} cm^{-1} for the LMCT bands and below 1.0 × 10^2 L mol^{-1} cm^{-1} for the d–d transitions, reflecting the Laporte-forbidden nature of the latter. The observed d–d transition energies and band positions are fully consistent with high-spin octahedral geometry for Fe(III) (d^5), Co(II) (d^7), and Ni(II) (d^8) centres as reported for

numerous analogous flavonoid and heterocyclic mixed-ligand complexes (Kumar et al., 2025; Abdou, 2025; Göktürk, 2025). Antimicrobial Studies

Table 1: Physicochemical properties of ligands and complexes

Ligands/Complexes	Colour	% Yield	Molecular Weight (g/mol)	Melting Point (°C)	Elemental Analysis % Calculated (% Found)			Conductivity (Ω^{-1} cm^2 mol^{-1})
					C	H	N	
Quercetin	Yellow	-	302.24	315.0	-	-	-	-
2-Aminothiazole	White	-	100.14	90.0	-	-	-	-
[Fe(QUE)(2-AMT)(H_2O)$_2$]	Black	70.12	492.24	330.0	43.92 (43.15)	3.28 (3.54)	5.69 (5.98)	18
[Co(QUE)(2-AMT)(H_2O)$_2$]	Black	69.23	495.33	325.0	43.42 (43.65)	3.37 (3.26)	5.51 (5.66)	20
[Ni(QUE)(2-AMT)(H_2O)$_2$]	Deep Orange	71.31	493.99	320.0	43.46 (43.67)	3.28 (3.26)	5.64 (5.66)	25

Table 2: FTIR spectral data of ligands and metal complexes (cm^{-1})

Compound	ν(OH)	ν(C=O)/ ν(C=N)	ν(C-O-H)	ν(C=C)	ν(M-O)/ ν(M-N)
Quercetin	3405	1664	1381.29	1610	--
2-Aminothiazole	3413	1520	--	--	--
[Fe(QUE)(2-AMT)(H₂O)₂]	3417	1651/ 1481	1358	1593	628–517
[Co(QUE)(2-AMT)(H₂O)₂]	3417	1635/ 1508	1385	1558	636–521
[Ni(QUE)(2-AMT)(H₂O)₂]	3417	1620/ 1508	1384	1431	698–621

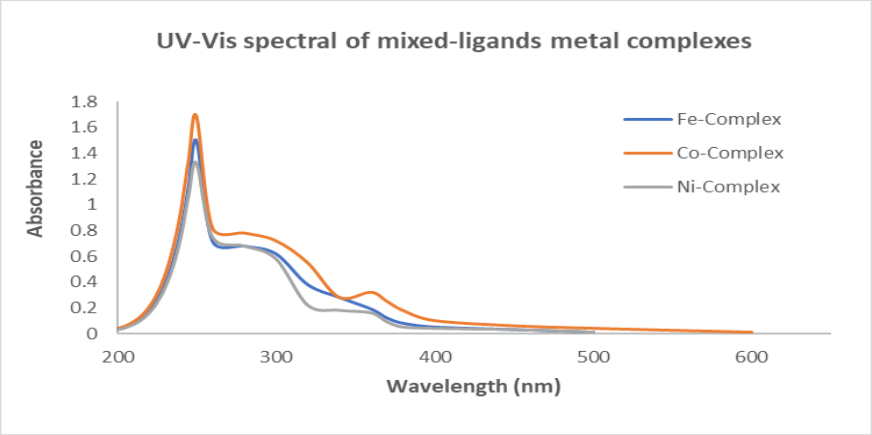

Figure 3: UV-Vis spectral of mixed-ligands metal complexes

Table 3: UV-Vis spectral data of ligands and metal complexes

Compound	λ_{max} (nm)	Assignment	ε ($L\ mol^{-1}\ cm^{-1}$)	Suggested Geometry
Quercetin	250, 370	π→π*, n→π*	3.2×10^4	–
2-Aminothiazole	255	π→π*	2.8×10^4	–
[Fe(QUE)(2-AMT)(H₂O)₂]	301, 405, 514	LMCT, $^6A_1g \rightarrow {}^4T_2g$, $^6A_1g \rightarrow {}^4T_1g$	3.8×10^3	Octahedral
[Co(QUE)(2-AMT)(H₂O)₂]	300, 406, 454, 503	LMCT, $^4T_1g(F) \rightarrow {}^4T_1g(P)$, ^4A_2g, $^4T_2g(F)$	4.1×10^3	Octahedral
[Ni(QUE)(2-AMT)(H₂O)₂]	300, 400, 501	LMCT, $^3A_2g(F) \rightarrow {}^3T_2g(P)$, $^3T_1g(F)$	3.5×10^3	Octahedral

The antimicrobial activities of quercetin (QUE), 2-aminothiazole (2-AMT), and their mixed-ligand metal complexes [M(QUE)(2-AMT)(H₂O)₂] (M = Fe, Co, Ni) were evaluated against representative Gram-positive, Gram-negative, and fungal strains: Staphylococcus

aureus, Escherichia coli, Klebsiella pneumoniae, Pseudomonas aeruginosa, and Aspergillus niger. The agar well diffusion method was employed, using dimethyl sulfoxide (DMSO) as the solvent control and ciprofloxacin (10 µg/mL) and fluconazole (10 µg/mL) as standard antibacterial and antifungal agents, respectively.All experiments were performed in triplicate, and results are presented as mean ± standard deviation (SD) (Figure 4). All assays were performed in triplicate, and results are expressed as mean ± standard deviation (SD). Statistical significance was determined by one-way analysis of variance (ANOVA) followed by Tukey's post-hoc test using GraphPad Prism 9.0. Differences in zone of inhibition between each complex and the free ligands, as well as among the three complexes, were highly significant ($p < 0.01$ for all pairwise comparisons across the five microorganisms). The order of activity [Co(II) > Ni(II) > Fe(III) > ligands] was statistically robust for all bacterial strains. Error bars illustrate the reproducibility of inhibition zone measurements, confirming a consistent biological response. Minimum inhibitory concentrations (MICs) were determined to quantify potency.

Zone of Inhibition and MIC Values

Both ligands displayed modest antimicrobial activity, with inhibition zones ranging from 10–14 mm. Upon coordination, activity increased markedly across all tested organisms. The Co(II) complex exhibited the strongest activity (22 ± 0.4 mm against *P. aeruginosa*, MIC = 75 µg/mL), comparable to the standard drug ciprofloxacin (24 ± 0.3 mm). The Ni(II) complex also showed notable inhibition (20 ± 0.5 mm against *E. coli*), while Fe(III) displayed moderate effects. Antifungal activity followed a similar trend, with the Co(II) complex again demonstrating superior inhibition (19 ± 0.6 mm against *A. niger*) (Sridevi & Madheswari, 2025; Alhussaini *et al.*, 2025).

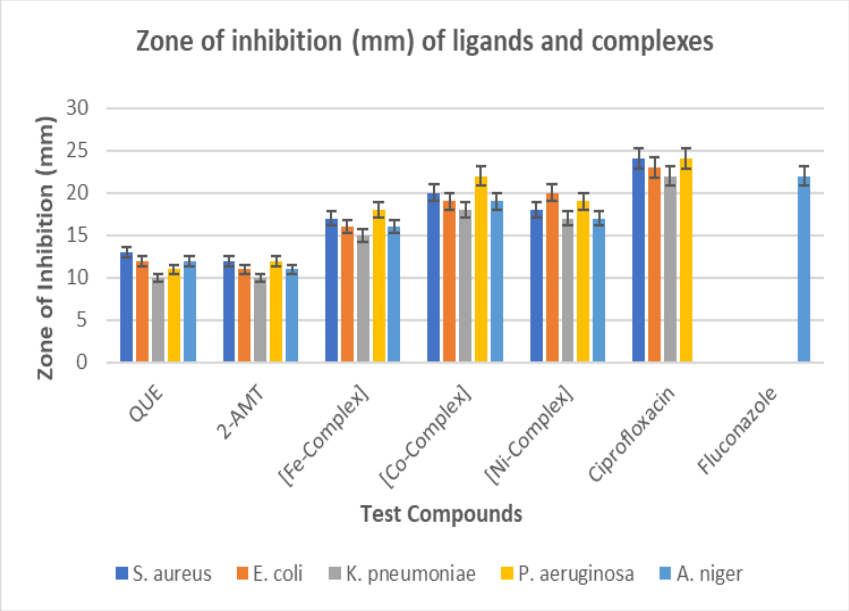

Figure 4: Zone of inhibition (mm) of ligands and complexes

Structure–Activity Relationship: The enhanced antimicrobial performance of the metal complexes relative to the free ligands is attributed to several synergistic factors:

1. **Increased lipophilicity:** Chelation reduces metal ion polarity and enhances permeability through the lipid membranes of microbial cells, in line with Tweedy's chelation theory [36].
2. **Metal–ligand synergy:** The presence of both oxygen (from QUE) and nitrogen (from 2-AMT) donor atoms creates mixed hard–soft coordination environments, stabilising the metal center and facilitating biointeraction.
3. **Redox activity and ROS generation:** Especially for Fe(III) and Co(II) species, redox cycling may generate reactive oxygen species (ROS) such as •OH and $O_2^{\bullet -}$, which induce oxidative stress and cell membrane damage [37].
4. **Membrane disruption and enzyme inhibition:** Coordination alters electronic distribution within the ligand system, potentially affecting microbial enzymes by binding to active-site residues or displacing essential metal ions [38].

Proposed Structure

The spectroscopic data suggest that the complexes adopt an octahedral geometry, with quercetin coordinating via its 3-hydroxy-4-carbonyl or 5-hydroxy-4-carbonyl sites and 2-aminothiazole via its endocyclic nitrogen. The presence of water molecules, inferred from broad ν(OH) bands, completes the coordination sphere. The proposed structure, [M(QUE)(2-AMT)$(H_2O)_2$], is depicted in Figure 5.

Conclusion

New mixed-ligand Fe(III), Co(II), and Ni(II) complexes of quercetin and 2-aminothiazole were successfully synthesized, spectroscopically characterized, and evaluated for antimicrobial activity. Spectroscopic evidence confirmed that quercetin coordinates through its carbonyl and phenolic oxygen atoms, while 2-aminothiazole binds via the endocyclic nitrogen, forming octahedral metal centers with two coordinated water molecules. The antimicrobial assays revealed that coordination significantly enhanced the biological activity of the ligands, following the order: [Co(QUE)(2-AMT)$(H_2O)_2$] > [Ni(QUE)(2-AMT)$(H_2O)_2$] > [Fe(QUE)(2-AMT)$(H_2O)_2$]

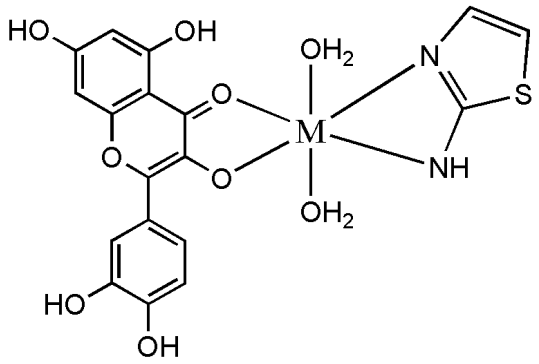

M = Fe, Co and Ni

Figure 5: Proposed octahedral structure of [M(QUE)(2-AMT)$(H_2O)_2$] complexes showing O,O- and N-donor coordination.

The superior activity of the Co(II) complex is attributed to its ability to undergo biologically accessible Co^{3+}/Co^{2+} redox cycling, which catalyses the generation of reactive oxygen

species (ROS) via Fenton-like chemistry (Co^{2+} + H_2O_2 → Co^{3+} + •OH + OH^-) and/or Haber–Weiss-type reactions inside microbial cells (AL-Ghamdi, 2025; Göktürk, 2025; Sadiq, 2023). Fe(III) can also participate in Fenton chemistry (Fe^{3+}/Fe^{2+}), but its high-spin d^5 configuration and higher reduction potential make this process less favourable under physiological conditions, resulting in moderate ROS production and lower activity. Ni(II) (d^8) possesses a stable +2 oxidation state with very limited redox activity in biological media; its antimicrobial effect therefore relies primarily on enhanced lipophilicity and direct inhibition of metalloenzymes rather than ROS generation (Alhussaini et al., 2025; Abdou, 2025). This clear gradation in redox behaviour (Co(II) >> Fe(III) > Ni(II)) directly correlates with the statistically validated activity order.The observed synergy between metal ions and the quercetin–thiazole ligand framework demonstrates the potential of such systems as prototypes for next-generation metal-based antimicrobials. Future studies should integrate density functional theory (DFT) calculations, molecular docking simulations, and cytotoxicity evaluations to rationalise binding interactions at the molecular level and assess biocompatibility. Such computational–experimental approaches will further elucidate the electronic factors underlying biological activity and guide the rational design of multifunctional coordination compounds with targeted therapeutic potential.

Table 4: Antibacterial activity (zone of inhibition, mm) at 200 µg/mL

Compounds	*S. aureus*	*E. coli*	*K. pneumoniae*	*P. aeruginosa*	*A. niger*	MIC (µg/mL)
QUE	13 ± 0.4	12 ± 0.5	10 ± 0.4	11 ± 0.3	12 ± 0.4	200
2-AMT	12 ± 0.5	11 ± 0.4	10 ± 0.3	12 ± 0.5	11 ± 0.4	175
[Fe(QUE)(2-AMT)(H_2O)$_2$]	17 ± 0.3	16 ± 0.4	15 ± 0.3	18 ± 0.5	16 ± 0.5	100
[Co(QUE)(2-AMT)(H_2O)$_2$]	20 ± 0.5	19 ± 0.4	18 ± 0.3	**22 ± 0.4**	**19 ± 0.6**	**75**
[Ni(QUE)(2-AMT)(H_2O)$_2$]	18 ± 0.4	20 ± 0.5	17 ± 0.5	19 ± 0.3	17 ± 0.4	90
Ciprofloxacin	24 ± 0.3	23 ± 0.3	22 ± 0.4	24 ± 0.3	–	50
Fluconazole	–	–	–	–	22 ± 0.4	50

References

Abdou, A. (2025). Synthesis, structural, DFT, in vitro biological exploration, and DNA interaction of new Ni(II) and Cu(II) mixed-ligand complexes featuring 2,2′-pyridine-2,6-diylbis(1H-benzimidazole) and 2-hydroxy-naphthaldehyde-based Schiff-base. *Applied Organometallic Chemistry, 39*(3), Article e7900. https://doi.org/10.1002/aoc.7900

Ai, F., & Lu, Y. C. (2025). Coordination chemistry in advanced redox-active electrolyte designs. *Nature Reviews Materials*. Advance online publication. https://doi.org/10.1038/s41578-024-00723-4

Al-Ghamdi, S. (2025). Structural and biological investigations of Fe(III) and Co(II) complexes with tryptophan and 2,2'-bipyridine: Implications for antibacterial and antifungal applications. *Journal of Umm Al-Qura University for Applied Sciences*. Advance online publication.

Alhussaini, M. S., Alyahya, A. A. I., & Al-Ghanayem, A. A. (2025). Selected thiazole-based M(II) complexes (M = Cu, Ni, or Co): Harnessing metal–ligand synergy against bacterial and fungal pathogens. *Dyes and Pigments, 224*, Article 112978. https://doi.org/10.1016/j.dyepig.2025.112978

Amin, M. A., Diker, H., Şahin, O., Varlikli, C., & Soliman, A. A. (2025). Synthesis, characterization, crystal structure, electrochemical and photoluminescence properties, DFT and molecular docking studies, and antimicrobial activities of two mononuclear nickel(II) complexes with pyrazole-derived ligands. *Journal of Molecular Structure, 1322*, Article 142763. https://doi.org/10.1016/j.molstruc.2025.142763

Ayinla, S. O., Rajee, A. O., Yusuff, K. O., Mbaeyi, G. G., Busari, H. K., & Obaleye, J. A. (2024). Synthesis and biological activity of mixed ligand metal complexes of 6-mercaptopurine-nicotinamide. *Caliphate Journal of Science and Technology, 6*(2), 217–229.

Bale, A. T., Osunniran, W. A., Ayipo, Y. O., Rajee, A. O., Bamigboye, M. O., & Obaleye, J. A. (2022). Heteroleptic transition metal complexes of eflornithine hydrochloride monohydrate: Synthesis, characterization, in silico and in vitro biological studies. *Manuscript submitted for publication*.

Bogatinovska, E. C., Najkov, K., Petrushevski, G., Geskovski, N., Koleva, V., & Stefov, V. (2025). Infrared and Raman spectra of racemic ibuprofen sodium dihydrate–Spectra-structure correlations. *Spectrochimica Acta Part A: Molecular and Biomolecular Spectroscopy, 339*, Article 126190. https://doi.org/10.1016/j.saa.2025.126190

Chagas, M. D. S. S., Behrens, M. D., Moragas-Tellis, C. J., Penedo, G. X., Silva, A. R., & Gonçalves-de-Albuquerque, C. F. (2022). Flavonols and flavones as potential anti-inflammatory, antioxidant, and antibacterial compounds. *Oxidative Medicine and Cellular Longevity, 2022*, Article 9966750. https://doi.org/10.1155/2022/9966750

Farajzadeh Öztürk, N., Akın, M., Şaki, N., & Bayır, Z. A. (2025). Design of active heterocycle-modified triangular silver nanoprisms: Antioxidants and antibacterial agents against *Staphylococcus aureus*. *Chemistry & Biodiversity*, Article e03433. https://doi.org/10.1002/cbdv.202403433

Garg, S. K., Shukla, A., & Choudhury, S. (2019). Polyphenols and flavonoids. In *Nutraceuticals in veterinary medicine* (pp. 187–204). Springer International Publishing. https://doi.org/10.1007/978-3-030-04624-8_13

Göktürk, T. (2025). Synthesis, characterization, BSA binding activity and ADME predictions of a new Co(II) complex with o-vanillin-based Schiff base ligand. *Mugla Journal of Science and Technology, 11*(1), 18–27.

Hadi, F. H., & Jamel, H. O. (2025). Evaluation of the effectiveness of palladium(II) complex with a new ligand derived from 2-hydrazinylbenzoxazole and 2-aminothiazole in anticancer activity. *Journal of Nanostructures, 15*(3), 896–907.

Hassan, S. S., Mohamed, E. F., Maged, K., Hassan, S., Hamad, A. O., Nasr, S., ... Saleh, A. M. (2025). Synthesis of new Cu(II), Ni(II), and Cd(II)-(N-glycyl-L-leucine) complexes as peptide metalloantibiotics for targeting pathogenic water with antioxidant effect

investigation. *Beni-Suef University Journal of Basic and Applied Sciences, 14*(1), Article 46. https://doi.org/10.1186/s43088-025-00456-7

Imai, K., Nakanishi, I., Ohkubo, K., Ohba, Y., Arai, T., Mizuno, M., ... & Fukuhara, K. (2017). Synthesis of methylated quercetin analogues for enhancement of radical-scavenging activity. *RSC advances*, *7*(29), 17968-17979.

Kapoor, K., Kaur, N., Sohal, H. S., Kaur, M., Singh, K., & Kumar, A. (2025). Drugs and Their Mode of Action: A Review on Sulfur-Containing Heterocyclic Compounds. *Polycyclic Aromatic Compounds*, *45*(1), 136-175.

Kasprzak, M. M., Erxleben, A., & Ochocki, J. (2015). Properties and applications of flavonoid metal complexes. *Rsc Advances*, *5*(57), 45853-45877.

Kumar, M., Singh, A. K., Singh, S., Singh, A. K., Rao, P. K., Yadav, R. K., ... & Tripathi, U. N. (2025). Exploration of iron (III) complexes with bidentate N, O-donor Schiff base ligands through synthesis, characterization, DFT, and antibacterial studies. *Journal of Molecular Structure*, *1319*, 139496.

McMills, L., Nyasulu, F., & Barlag, R. (2014). *Magnetic Susceptibility of Coordination Compounds in the General Chemistry Laboratory*. *2*(2), 11–14. http://article.sapub.org/pdf/10.5923.j.jlce.20140202.01.pdf

Mohammed, N. A., Mohammed, M. Y., Alheety, M. A., Majeed, A. H., & Yahya, M. Z. A. (2025). Thermodynamic and Kinetic Analysis of Hydrogen Capture in a Homobinuclear Palladium (II) Complex. *Energy Storage*, *7*(5), e70248.

Obaleye, J.A., Lawal, A., Rajee, A.O., Babamale, H.F. & Shittu, F.B. (2014). Synthesis, Characterization and Antimicrobial Activity of mixed Amodiaquine and Sulphadoxine mixed Ligands – metal Complexes. *Nigerian Journal of Biochemistry and Molecular Biology – NJBMB*: 29(2):170-179.

Pravin, N., & Raman, N. (2013). DNA interaction and antimicrobial activity of novel tetradentate imino-oxalato mixed ligand metal complexes. Inorganic Chemistry Communications, 36, 45-50.

Rajee, A. O., Ayinla, S. O., Simon, N., Yusuff, O. K., Lawal, M., & Busari, H. K. (2022). Synthesis of thiamine HCl–metal complex of Zn (II) ion and the structural elucidation using single crystal X-ray crystallography (SCXRD), density functional theory (DFT) and biological studies. *Chemistry Africa*, *5*(5), 1377-1386.

Rajee, A. O., Babamale, H. F., Aliyu, A. A., Lawal, A., Ayinla, S. O., Osunniran, W. A., & Musa, I. (2020). Synthesis, Structural Elucidation and Antimicrobial Activity of Metal (II) Polypyridyl Complexes of 2-Amino-4-(Methylthio) Butanoic Acid. *Fountain Journal of Natural and Applied Sciences*, *9*(1).

Rajee, A. O., Babamale, H. F., Lawal, M., Ayinla, S. O., Lawal, A., & Obaleye, J. A. (2018). Artemether-Lumefantrine Mixed Ligand Complexes: Synthesis and in vitro Antiplasmodial Activity Studies.

Rajee, A. O., Obaleye, J. A., Louis, H., Ayinla, S. O., Aliyu, A. A., Osunniran, W. A., ... & Manicum, A. L. E. (2024). Ruthenium polypyridyl complexes with hydroxypyridine: experimental, DFT studies, and in silico antitubercular activity investigation. *Chemistry Africa*, *7*(2), 835-847.

Ramzan, N., Butt, H., Azeem, M., Hanif, M., Mahmood, K., Rehman, S., ... & Jabeen,

M. (2025). Therapeutic applications of quercetin-metallic complexes: a review. *BioMetals*, 1-22.

Refat, M. S., Hamza, R. Z., Adam, A. M. A., Saad, H. A., Gobouri, A. A., Al-Salmi, F. A., ... & El-Megharbel, S. M. (2021). Potential therapeutic effects of new ruthenium (III) complex with quercetin: characterization, structure, gene regulation, and antitumor and anti-inflammatory studies (RuIII/Q novel complex is a potent immunoprotective agent). *Crystals*, *11*(4), 367.

Sadiq, I. Z. (2023). Free radicals and oxidative stress: Signaling mechanisms, redox basis for human diseases, and cell cycle regulation. *Current molecular medicine*, *23*(1), 13-35.

Selvaraj, C., Rudhra, O., Alothaim, A. S., Alkhanani, M., & Singh, S. K. (2022). Structure and chemistry of enzymatic active sites that play a role in the switch and conformation mechanism. *Advances in Protein Chemistry and Structural Biology*, *130*, 59-83.

Sridevi, N., & Madheswari, D. (2025). Synthesis, characterization, and biological evaluation of Schiff base ligand and their metal complexes: implications for coordination chemistry and biomedical applications. *Polyhedron*, 117796.

Stefanache, A., Miftode, A. M., Constantin, M., Bogdan Goroftei, R. E., Olaru, I., Gutu, C., ... & Lungu, I. I. (2025). Noble Metal Complexes in Cancer Therapy: Unlocking Redox Potential for Next-Gen Treatments. *Inorganics*, *13*(2), 64.

Thakur, S., Kumar, D., Jaiswal, S., Goel, K. K., Rawat, P., Srivastava, V., ... & Dwivedi, A. R. (2025). Medicinal chemistry-based perspectives on thiophene and its derivatives: exploring structural insights to discover plausible druggable leads. *RSC Medicinal Chemistry*, *16*(2), 481-510.

Tweedy, B. G. (1964). Plant extracts with metal ions as potential antimicrobial agents. Phytopathology, 55(8), 910-914.

Woźnicka, E., Miłoś, A., Zapała, L., Kosińska-Pezda, M., Lecka-Szlachta, K., & Byczyński, Ł. (2025). Design and Characterization of Mn (II), Co (II), and Zn (II) Complexes with Chrysin: Spectroscopic, Antibacterial, and Anti-Biofilm Insights. *Processes*, *13*(8), 2468.

Yaraki, M.T., Zahed Nasab, S., Zare, I., Dahri, M., Moein Sadeghi, M., Koohi, M., & Tan, Y. N. (2022). Biomimetic metallic nanostructures for biomedical applications, catalysis, and beyond. *Industrial & Engineering Chemistry Research*, *61*(22), 7547-75933.